J. Water Environ. Nanotechnol., 4(3): 213-226 Summer 2019

ORIGINAL RESEARCH PAPER

Polysulfone nanocomposite membrane embedded by silanized nanodiamond for removal of humic acid from water

Atefeh Tizchang[1,2], Yoones Jafarzadeh[1,2,*], Reza Yegani[1,2], Elham Shokri[3]

[1] *Faculty of Chemical Engineering, Sahand University of Technology, Tabriz, Iran*
[2] *Membrane Technology Research Center, Sahand University of Technology, Tabriz, Iran*
[3] *Department of Chemical Engineering, University of Bonab, Bonab, Iran*

Received: 2019-05-23 Accepted: 2019-07-14 Published: 2019-08-01

ABSTRACT

In this study, polysulfone (PSf) nanocomposite membranes embedded with functionalized nanodiamond (ND) were prepared via Non-Solvent Induced Phase Separation (NIPS) method. ND nanoparticles were silanized by using the esterification reaction of hydrolyzed vinyltrimethoxysilane (VTS) in alcoholic solution in order to enhance the compatibility between ND and PSf. Fourier Transform Infrared Spectroscopy (FTIR) analysis revealed that ND nanoparticles were successfully functionalized by silane groups. Nanocomposite membranes were then prepared with different percentages of silanized NDs (SNDs). The membranes were characterized using a set of analyses and the results showed that the addition of SNDs up to 1.0 wt.% resulted in an increase in hydrophilicity, water content, porosity and water flux of membranes. Moreover, Scanning Electron Microscopy (SEM) images indicated that the membrane with 1.0 wt. % nanoparticles had more pores on the membrane surface with smaller average pore size in comparison to other membranes. Antifouling properties of the membrane was also investigated in filtration of humic acid solution and the results showed that reversible fouling and flux recovery of membranes increased at the presence of SNDs.

Keywords: *Polysulfone, Functionalization, Nanodiamond, Fouling, Nanocomposite.*

How to cite this article
Tizchang A, Jafarzadeh Y, Yegani R, Shokri E. Polysulfone nanocomposite membrane embedded by silanized nanodiamond for removal of humic acid from water. J. Water Environ. Nanotechnol., 2019; 4(3): 213-226.
DOI: 10.22090/jwent.2019.03.004

INTRODUCTION

The presence of humic acid (HA) as a natural organic matter (NOM) in surface water causes health problems because it reacts with disinfectants during the water treatment process and form toxic and carcinogenic disinfection by-products (DBPs) [1, 2]. Therefore, it is necessary to remove HA from water using effective treatment processes. Chemical coagulation/flocculation, electrocoagulation, oxidation, adsorption, and membrane filtration methods have been used for HA removal. During the last decades, membrane filtration has been considered as an efficient method because of its low cost, high efficiency and less energy requirement [3, 4]. Ultrafiltration (UF) membranes which are appropriate for HA removal, can be prepared using a wide range of polymers including polyethersulfone (PES), cellulose acetate (CA), polyvinylidene fluoride (PVDF) and polysulfone (PSf). Among them, PSf is widely employed for preparation of UF membrane due to its excellent mechanical, chemical and thermal properties [5, 6]. However, the hydrophobic nature of PSf results in fouling and flux decline during treatment process of surface water containing NOMs [7-9]. Increasing the hydrophilicity of membranes by surface or bulk modification has been offered to reduce membrane fouling. Incorporation of inorganic nanoparticles into polymer matrix of membranes is a kind of bulk modification method to improve the hydrophilicity

* Corresponding Author Email: *yjafarzadeh@sut.ac.ir*

and antifouling properties of the membrane [8]. The effects of incorporating different nanoparticles like graphene oxide (GO) [10], organoclay [5], GO-TiO_2 [11] and GO-SiO_2 [12] into the PSf polymeric matrix have been investigated. Most recently, nanodiamond (ND), an emerging carbon nanomaterial, has gained lots of attention especially in nanocomposite membranes due to its high surface area, hydrophilicity, biocompatibility, non-toxicity and different functional groups on the surface [13, 14]. Therefore, ND can be a proper choice to be embedded in the PSf matrix to overcome the hydrophobic nature of it. Despite this, unmodified NDs suffer from agglomeration and non-uniform distribution in polymer matrix. Therefore, an increasing number of researches are being carried out to reduce the agglomeration of ND nanoparticles and improve their performance, especially by surface modification due to the presence of different functional groups on the surface. One of the most common techniques for functionalization of ND nanoparticles to be embedded in polymer matrix is silanization [15, 16]. Jeong et al. used modified ND with (3-methacryloxypropyltrimethoxysilane) to fabricate nanodiamond/acrylic resin composite [17]. They showed that incorporating modified ND into composite leads to improvement of optical and mechanical properties. In another study, Dolmatov investigated the effect of modified ND with silane coupling agent on the properties of composite based on elastomer and polymer matrices [18]. They showed that dispersibility of NDs improved by silanizationn which causes to improve the properties of elastomer composite. Hajiali et al. modified ND with different degrees of vinyltrimethoxysilane and showed that ND with maximum degree of silane coupling agent had more stable suspension in hydrophobic medium and better interaction with polydimethylsiloxane [19].

To the best of our knowledge, there is no report in the literature about PSf membranes embedded with silanized nanodiamonds to be used in the MBR system. In this study, vinyltrimethoxysilane was used as silane coupling agent to overcome the insufficient dispersion of ND nanoparticles in the PSf matrix. Silanized nanodiamonds (SNDs) were then employed to fabricate PSf/SND membranes via NIPS method. The influence of the different amounts of SND loading in the membrane structure, performance, morphology and hydrophilicity of resultants membranes were investigated. In the following, the fouling mechanisms of the membranes during the filtration of HA were analyzed by using Hermia (classic) and combined fouling models. Finally, pre-coagulation process using aluminum-based coagulant (PAC) was used to increase the HA rejection.

MATERIALS AND METHODS

Materials

Udel P-1700 polysulfone was purchased from Solvay Advanced Polymer LLC and used as the polymer. The pristine detonation ND nanoparticles with a phase purity higher than 95 were procured from Nabond technology Co., Ltd., China. The average diameter and specific surface area of ND nanoparticles were 5 nm and 282.8 m^2g^{-1}, respectively. N-Methyl-2-Pyrrolidon (NMP) from Daejung was used as the solvent, polyethylene glycol (PEG) (Mw = 20,000 (g/gmol)) as pore-forming and Vinyltrimethoxysilane (VTS) with the purity of 97% from Merck was used for silane functionalization of ND. The following materials were used without further purification: ethanol (99.8% Sigma Aldrich), acetone (99% Merck) and acetic acid (99.85%) Sigma Aldrich). Deionized (DI) water was used as a nonsolvent to induce phase inversion and also as a medium to measure the pure water flux.

Silanization of ND

Surface modification of ND was first carried out by using the thermal oxidation of ND at 425°C to enhance the surface carboxyl content. Carboxylated ND as COOH-ND was then reacted with hydrolyzed VTS by esterification method leading to SND. The silanization was performed by preparing 80 ml solution of distilled water/ethanol (20:80 v/v) and adjusting its pH to 3.5-4.5 by adding acetic acid. The desired amount of VTS was then added to the solution followed by stirring at ambient temperature for 30 min. This process leads to hydrolysis of the silane. According to the literature, the best weight ratio of (VTS/COOH-ND, w/w) is 5:1, so a specific amount of COOH-ND (0.3g) was added to the solution and dispersed by an ultrasonic bath (120W, 28 kHz) for an hour [19]. Next, the mixture was stirred for 4h at 65°C using a hot plate. Then, the suspension was placed in an oven at 120°C for 4h developing the esterification of silanol groups on ND surface and evaporation of water/ethanol solution. Finally, SND was washed

out sequentially with acetone and distilled water and dried in an oven at 120°C for around 12 h.

Characterization of SND

The chemical structure of SND was studied by Fourier transform infrared spectroscopy (FTIR) with a VERTEX 70 FTIR spectrometer (Bruker, Germany) within the wavelength of 400-4000 cm^{-1}.

Preparation of neat and nanocomposite membranes

Neat and nanocomposite PSf membranes were prepared by using nonsolvent induced phase separation (NIPS) method. Table 1 presents the compositions of casting solutions. In the case of the composite membrane, the pre-determined amount of SND was dispersed into NMP by applying sonication. Subsequently, PSf and PEG were added to the dispersion and the mixture was stirred by a mechanical stirrer at a temperature of 60 ℃ to give homogenous solution. To prepare defect free membrane, enough time was given for bubbles to be completely released. A portion of the resulting solution was poured onto flat plate glass and spread out with an automatic casting knife at the speed of 10 mm/s and a gap of 150 μm. The glass plate together with the cast film was immersed in a water bath to initiate phase inversion immediately. The obtained membranes were thoroughly rinsed with deionized water and dried at room temperature to remove the residual solvent. Neat PSf membrane without inorganic filler was also prepared according to the same method mentioned above.

Characterization of membranes

Pure water flux (PWF)

Pure water flux of membranes was determined using a fabricated dead-end filtration system with 5cm^2 of effective membrane area. The feed was pressurized by nitrogen gas cylinder connected to the feed tank. To avoid any compaction, the membranes were compacted for 30 min at 2 bar. Then permeation experiment was subsequently carried out at 1.5 bar and after reaching steady state, water flux was calculated through the Eq. (1):

$$J_0 = \frac{M}{A\,t} \tag{1}$$

Where J_0 (Kg/m^2.h) is pure water flux, M is collected mass of water (Kg), A is effective membrane area (m^2) and t is sampling time (h).

Contact angle

The surface hydrophilicity of the prepared membranes was evaluated by measuring the contact angle between the membrane surface and water droplet using a contact angle goniometer (PGX, Thwing-Albert Instrument Co.). DI water was used as the probe liquid for all measurements. The results were the average of at least five tests at different locations on the membrane surface.

Membrane porosity and water content

Water content (WC) tests were conducted to study the adsorption capability of water to membranes. In this test, after soaking membranes in water for 24 h, the membranes were weighed (W_{wet}) followed by mopping with blotting paper. The wet membranes were placed in a vacuum drier at 50°C for 24 h and the dry weights (W_{dry}) of the membranes were determined according to the method developed by Sivakumar et al. The percent of WC was calculated through the following Eq. (2) [20, 21]:

$$WC\,\% = \frac{W_{wet} - W_{dry}}{W_{wet}} \times 100 \tag{2}$$

The porosity of prepared different membranes was calculated by Eq. (3) [10]:

$$\varepsilon(\%) = \frac{(W_w - W_d)/D_w}{(W_w - W_d)/D_w + W_d/D_p} \times 100 \tag{3}$$

Where ε is the porosity of membrane (%), W_w and W_d are the wet and dry sample weight (g), respectively. Meanwhile, D_w is the density of water at 25°C (0.998 g.cm^{-3}) and D_p is the density of polymer (1.24 g.cm^{-3}).

Morphology and pore size distribution

The morphology of membranes was investigated by MIRA XM field Emission Scanning Electron Microscope (FE-SEM). Cross-section samples were

Table 1. Casting solution composition of neat and nanocomposite PSf membranes

Membrane	SND/PSf ratio (wt/wt %)	PSF (wt%)	PEG (wt%)	NMP (wt%)	SND (wt%)
PSf	-	15	10	75	-
PSf/SND/0.5	0.5	14.925	10	75	0.075
PSf/SND/1.0	1	14.85	10	75	0.15
PSf/SND/1.5	1.5	14.775	10	75	0.225

prepared by fracturing the membranes in liquid nitrogen and were coated with gold by sputtering before observation to make them conductive. SEM device was equipped with dispersive X-ray analysis (EDX) detector to inspect the existence as well as dispersion of SND nanoparticles in the membranes. Pore size distribution was estimated by analyzing the surface SEM images of membranes using ImageJ Analyzer software.

Mechanical strength

Mechanical strength of membranes was measured by a tensile testing machine (STAM-D, SANTAM, Iran). All samples for mechanical testing were in a rectangular shape and the testing speed was adjusted at 10 mm/min. Each membrane was tested at least 3 times and averaged values were reported.

Filtration experiment

In order to evaluate the effect of SND on the membrane fouling behavior, filtration of HA solution was performed by using the dead-end filtration system. HA solution was prepared by dissolving 0.4 g of HA in 400 ml of water at the pH of 6 and stored in the refrigerator (4°C) before use.

After measuring pure water flux (J_0), the filtration system was filled with prepared HA solution and the permeate flux profile was recorded every 10 min. After 180 min of HA filtration and fouling, PWF measured and recorded as J_1. Then, the cake layer on the membrane was rinsed and removed mechanically by a sponge. Afterward, pure water was again passed through the membrane and PWF (J_2) was calculated. To investigate the fouling behavior of the fabricated membranes, the flux recovery ratio (FRR), reversible fouling ratio (RFR), irreversible fouling ratio (IFR) and total fouling ratio (TFR) of the membranes were calculated by using the following equations[22]:

$$\mathrm{FRR}\,(\%)=\left(\frac{J_2}{J_0}\right)\times 100 \tag{4}$$

$$RFR\,(\%)=\left(\frac{J_2-J_1}{J_0}\right)\times 100 \tag{5}$$

$$IFR\,(\%)=\left(\frac{J_0-J_2}{J_0}\right)\times 100 \tag{6}$$

$$TFR\,(\%)=\left(\frac{J_0-J_1}{J_0}\right)\times 100 \tag{7}$$

In order to measure the membrane rejection, the HA concentrations of feed and permeate solutions were determined by using a UV spectrophotometer (Bio Quest CE2501) and the HA rejection of membrane was calculated by using Eq (8):

$$R\,(\%)=\left(1-\frac{C_p}{C_f}\right)\times 100 \tag{8}$$

Where R(%) is the rejection percentage, C_p and C_f are permeate and feed concentrations, respectively.

Analysis of the fouling mechanism

To better understand the fouling mechanism of the membranes under the condition of constant pressure filtration, Hermia proposed the following mathematical form for flux decline:

$$\frac{d^2t}{dV^2}=k\left(\frac{dt}{dV}\right)^m \tag{9}$$

Where V is the cumulative volume of filtrate, t the time of operation, and m & k are kinetics parameters. The permeate flux is presented as:

$$j=\frac{1}{A}\frac{dV}{dt} \tag{10}$$

Using the flux equation, Eq (9) can be written as:

$$\frac{dJ}{dt}=-kJ(AJ)^{2-m} \tag{11}$$

The linear forms of flux expressions and analytical solutions for each value of m which characterize the fouling model are listed in Table S1 (given in supplementary data).

In addition to Hermia, constant pressure combined models of membrane fouling were also used. In combined models, the assumption is that the two fouling mechanisms are independent and will occur throughout the filtration[23]. A summary of the constant pressure combined fouling models are presented by Bolton and is provided in Table S2 (given in supplementary data)[24].

RESULTS AND DISCUSSIONS

Characterization of SND

Fig. 1 represents the surface chemistry of pure ND, carboxylated ND (ND-COOH) and silanized ND (SND) by FTIR spectra. For ND, the absorption bands at 2923 and 2852 cm^{-1} are assigned to the asymmetric and symmetric stretching vibration of C-H band, respectively [25]. The absorption bands

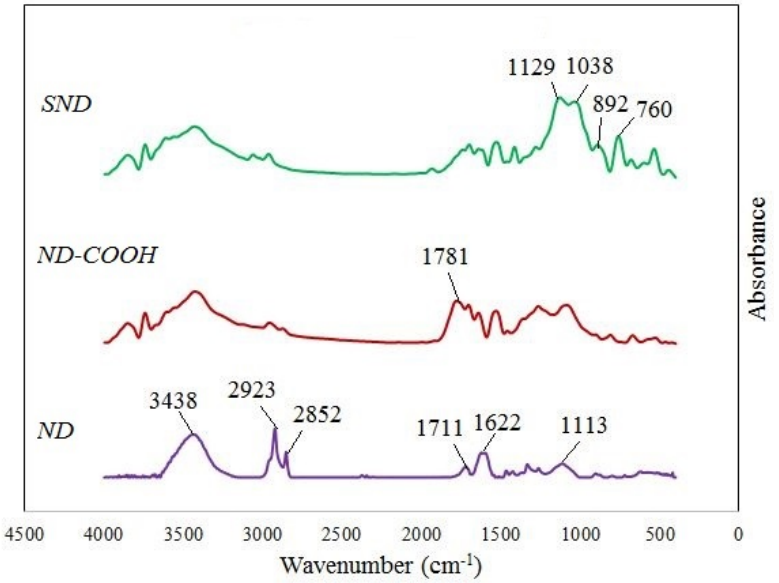

Fig. 1. FTIR spectra of pure ND, ND-COOH, and SND.

Table 1. Casting solution composition of neat and nanocomposite PSf membranes

Membrane	Contact angle, degree	Porosity (%)	Water content (%)	PWF ($Kg/m^2.hr$)
PSf/SND (0.0 wt%)	83.10	59.47	54.16	410.41
PSf/SND (0.5 wt%)	77.57	60.23	54.94	552.04
PSf/SND (1.0 wt%)	76.44	71.64	67.11	905.075
PSf/SND (1.5 wt%)	78.86	48.76	43.42	585.551

at 3438 and 1622 cm^{-1} can be attributed to O-H groups [26]. The spectrum showed another band from oxygen-containing functional groups at 1711 and 1113 cm^{-1} which are assigned to the stretching vibration of C=O and C-O-C groups, respectively. Also for ND-COOH, absorption band of C=O is shifted from 1711 cm^{-1} to 1781 cm^{-1} is attributed to the conversion of oxygen-containing groups like ketone, alcohol, and ester to carboxylic group [27]. For the SND nanoparticles absorption band at 760 cm^{-1} and 1038 cm^{-1} are attributed to Si-C and Si-O-Si respectively [28]. The absorption band at 1129 cm^{-1} is attributed to Si-O-C and is a confirmation of the presence of silane functional groups on ND surface[19]. Also the band at 892 cm^{-1} represents unreacted SiOR groups in organosilane [29].

Characterization of membranes

Contact angle measurements

The surface hydrophilicity of the membranes was examined by measuring the contact angle between the membrane surface and water droplets. A decrease in surface contact angle is an index for improvements in the hydrophilicity of the membranes [8, 30]. The results of the contact angle of membranes listed in Table 2 revealed that contact angle of membranes decreases continuously with increasing SNDs content in the membranes. As shown in Fig. 1, SNDs have carboxyl groups on their surface which increase the interaction with water molecules and subsequently, enhances the hydrophilicity of membranes [31]. Furthermore, comparing the contact angle of PSf/SNDs nanocomposite membranes confirms that increasing the hydrophilic groups on the membrane surface leads to decrease contact angle. However, when the SNDs content increases to 1.5 wt%, contact angle increased which may be attributed to the agglomeration of the particles and less presence of hydrophilic nanoparticles on the surface of the membrane.

Membrane morphology and pore size distribution

The SEM images of the top surface of the neat and SNDs incorporated PSf membranes were shown in Fig. 2 . It can be seen that with the addition

of SNDs (≤1.0 wt%), more pores with smaller sizes appear on the membrane surface which may play a favorable role on membrane flux and fouling properties. According to the results reported by Gohari et al., hydrophilic nanoparticles can act as a disperser of nonsolvent into small droplets in the top skin layer, which resulted in a large number of small pore sizes [32]. However, when the addition of SND further increases (1.5 wt%), the top surfaces gradually become dense (Fig.2 d). This result can be attributed to agglomeration and cluster formation of NDs and consequently non-uniform dispersion of nanoparticles in higher concentrations[15].

Fig. 2 also shows the cross-section morphology of the ultrafiltration membranes. All membranes possess a typical asymmetric structure with a dense top layer and fully developed macrovoids at the bottom. However, addition of SNDs causes to increase the size of macrovoids and the thickness of dense layer. It should be noted that both thermodynamic and kinetic aspects play a role in the structure of membrane as the amount of SNDs was increased. The differences of the cross-section structures are likely due to the change in the viscosity of casting solution, which results from the addition of SNDs [33, 34]. Generally, the increase of skin layer is attributed to the decrease of exchange rate between solvent and nonsolvent during phase separation [35]. Furthermore, the formation of macrovoids can be suppressed by increasing the viscosity of the casting solution which decreases the ability of nonsolvent to diffuse in the cast film.

The pore size distribution (PSD) of membranes can also be useful in understanding the effect of

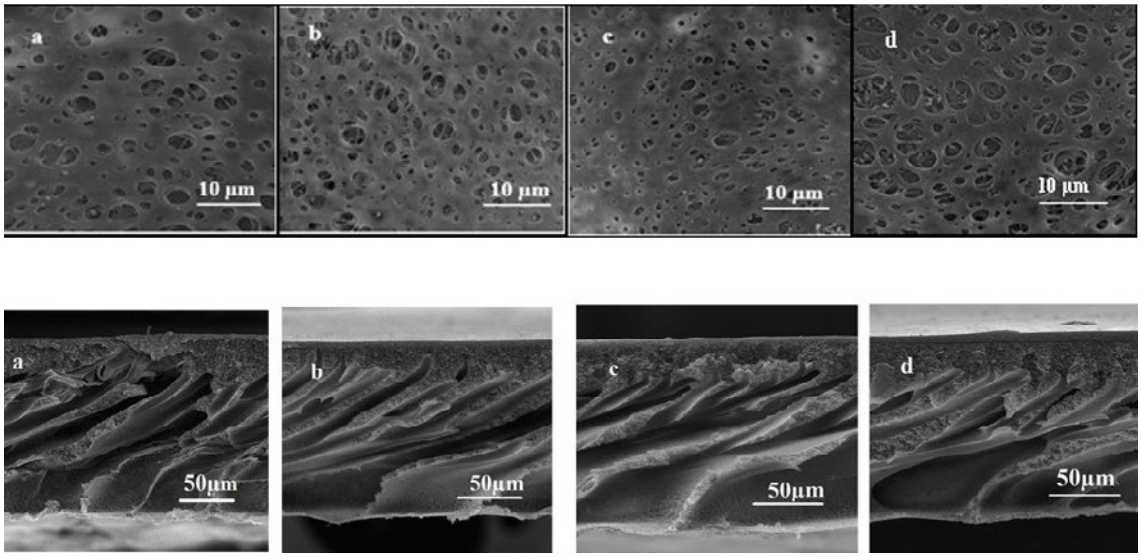

Fig. 2. SEM images of top surface (top) and cross-sectional (bottom) of: (a) PSf, (b) PSf/SND (0.5 wt%) (c) PSf/SND (1.0 wt%), (d) PSf/SND (1.5 wt%)

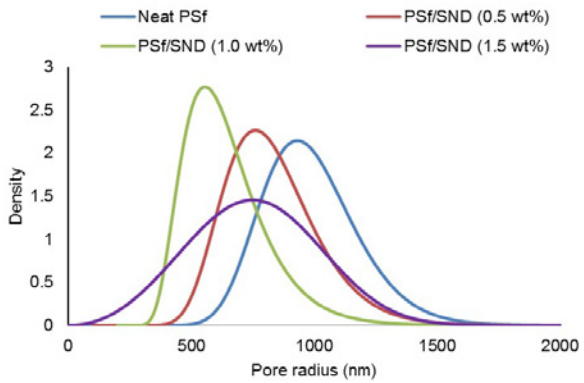

Fig. 3. The pore size distribution of membranes.

SNDs on the morphology of prepared membranes. The PSD of the membranes are shown in Fig. 3, and it can be seen that by embedding the NPs into the polymeric matrix, the PSD is shifted towards smaller pores until 1.0 wt% which is in accordance with the SEM surface images of membranes. The difference in PSD of membranes can be attributed to the phase inversion step of casting solutions. The presence of SND up to 1 wt% increased the rate of solvent and non-solvent exchange in the phase inversion process so it improved the porosity of the membrane. However, addition of more than 1 wt% SND caused agglomeration of SNDs which may decrease solvent-nonsolvent exchange rate. In addition, the higher content of SND nanoparticles in dope solution increased its viscosity and consequently, delayed phase inversion and decreased the porosity. Therefore, the number of pores on the surface of the membrane decreased but mean pore radius increased.

In order to investigate the existence of SNDs on the surface of the membranes, the EDX analysis was carried out based on Si element and obtained results are presented in Fig. 4. A peak observed around 1.7 keV belongs to Si in SNDS and the peak around 2.5 keV belongs to sulfur which comes from PSf. To examine if SND is well dispersed in the membrane matrix, EDX mapping test was done on the PSf/SND (1.0 wt%) membrane and obtained results are shown in Fig. 4. According to the images, it is obvious that SNDs are perfectly distributed in the polymer matrix.

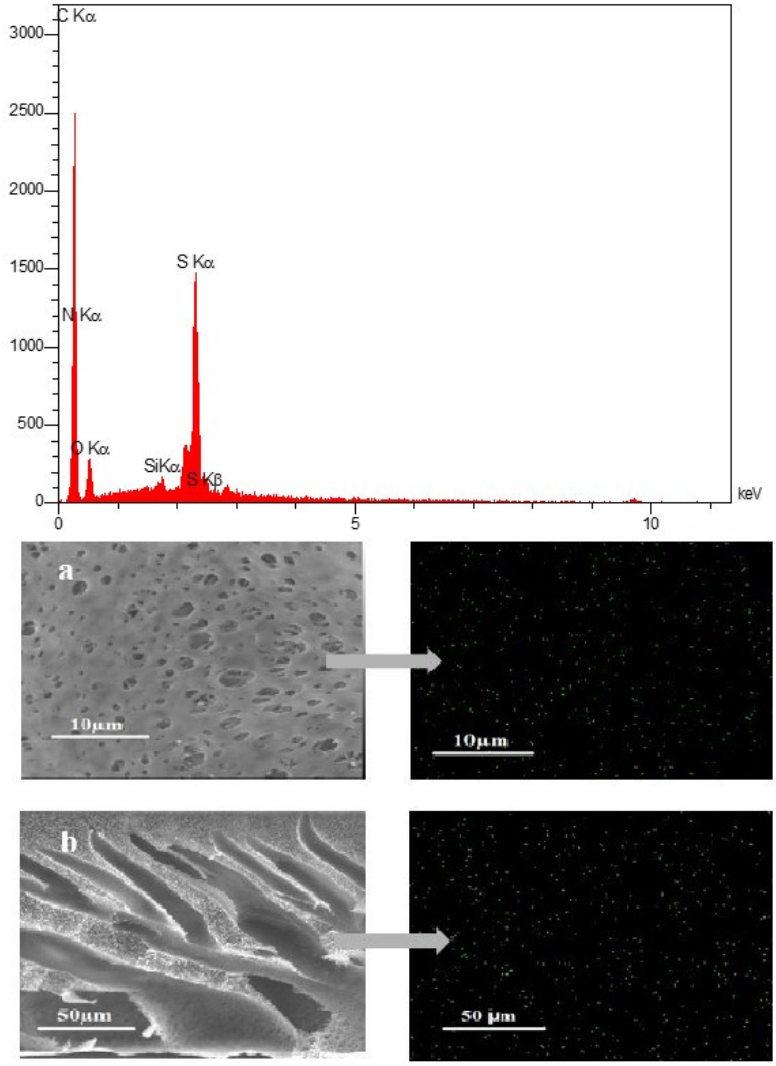

Fig. 4. The EDX result of PSf/SND (1.0 wt%) membrane (top) and Backscattered SEM of PSf/SND (1.0 wt%) membrane (a) surface, (b) cross-section (bottom)

Table 2. Contact angle, porosity, water content and PWF results for neat and nanocomposite PSf membranes.

Membrane	Contact angle, degree	Porosity (%)	Water content (%)	PWF ($Kg/m^2.hr$)
PSf/SND (0.0 wt%)	83.10	59.47	54.16	410.41
PSf/SND (0.5 wt%)	77.57	60.23	54.94	552.04
PSf/SND (1.0 wt%)	76.44	71.64	67.11	905.075
PSf/SND (1.5 wt%)	78.86	48.76	43.42	585.551

Pure water flux

Pure water flux (PWF) and pores size distribution are often regarded as two important factors for porous membranes. The number and size of the pores on the membrane surface have a direct relationship with PWF. As depicted in Table 2, neat PSf exhibited the lowest PWF among the fabricated membranes and for PSf/SND (1.0 wt%), water flux reached its peak value (905.072 $Kg.m^{-2}h^{-1}$) which is about 2.2 times higher than neat PSf membrane. The increase of PWF can be related to the hydrophilicity of the membranes. Hydrophilic surfaces tend to absorb water on the membrane surface that improves pure water flux of the membrane. Moreover, as shown in SEM images, the number of surface pores as well of pores increased as the content of SNDs increased which provides more paths for water permeation.

Any further increase in SNDs contents up to 1.5 wt % reduces the PWF due to the agglomeration of NDs on the membrane surface [36]. The obtained results show great consistency with SEM images, confirming that the SNDs content of 1.0 wt % is the optimum value to incorporate in PSf membrane.

Porosity and water content

The overall porosity and water content information of the membranes were presented in Table 2. The results of the porosity measurement showed that porosity of PSf membrane containing 1.0 wt% SND elevated to 71.64% from 59.47% for PSf membrane. The improved membrane porosity resulting from incorporating SNDs in the PSf matrix is most likely due to the wider marcrovoids at the bottom of the membranes as evidenced from SEM images. It is also known that the improved porosity of the membranes can enhance the water content by detaching of polymer chains from SND surface, causing interface voids. However higher contents of SNDs do not yield further increase in the porosity and water content of the nanocomposite membranes because of the particle agglomeration as mentioned before.

Mechanical strength

Variation of mechanical strength and elongation at break with nanoparticle concentration are presented in Fig. 5. As can be seen, with increasing the amount of SNDs into the polymer matrix, there has been no great difference in mechanical strength. Actually as mentioned above, although nanocomposite membranes containing up to 1.0 wt% have improved porosity compared to the neat membrane, on the other hand, the mechanical strength has not been changed and has stayed stable which is probably due to the good interaction between the polymeric matrix and SNDs. In other words by increasing the porosity it was anticipated that mechanical strength of the membranes will diminish, but it did not occur because well dispersion of SND within PSf increased reinforcement effect and compensated

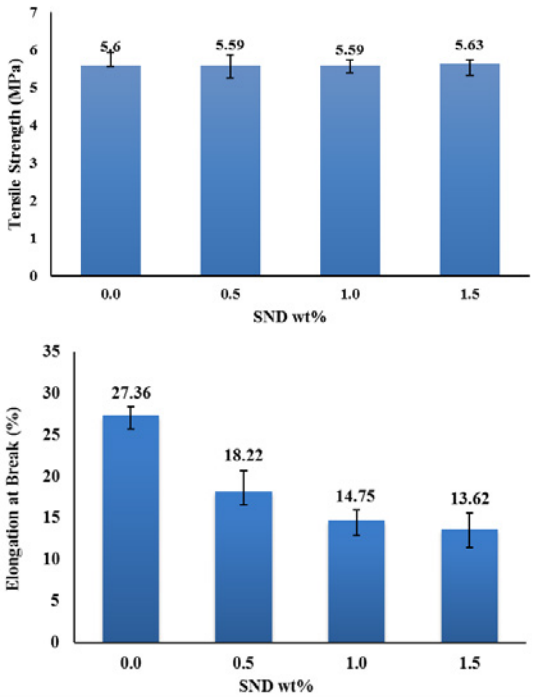

Fig. 5. Mechanical properties of pure and nanocomposite PSf membranes; tensile strength (top) and elongation at break (bottom)

the effect of porosity decline and consequently, tensile strength was not decreased considerably. On the other hand by addition of nanoparticles into the polymer matrix, the elongation at break of the nanocomposite membranes have decreased which is a direct consequence of increase in porosity.

Fouling analysis and membrane performance

Fig. 6 represents the fabricated membranes flux decline during HA filtration. As it can be seen elementary fluxes of all the nanocomposite membranes are higher than the neat PSf membrane and when the amount of SND nanoparticles reaches to 1 wt% the flux of HA filtration has elevated so dramatically. On the other hand, during the time, membranes with high flux of HA filtration will encounter more fouling problem that causes a significant decline of flux in last minutes of filtration process. This can be attributed to the hydrophilicity of 1.5 wt. % membrane. As shown in Table 2, contact angle increased from 76.4° for 1.0 wt. % SND membrane to 78.8° for 1.5 wt. % SND membrane meaning that the hydrophilicity of the latter is less than the former. It has been accepted that hydrophobic membranes are more susceptible to fouling and therefore, filtration flux 1.5 wt. % SND membrane is less than 1.0 wt. % SND membrane.

In order to obtain the information about antifouling properties of the membranes, fouling parameters including TFR, RFR, IFR and FRR of membranes were calculated. Table 3 shows a summary of these parameters for neat and nanocomposite membranes. The results show that neat PSf has the highest TFR, indicating that this membrane was fouled easily by HA. Addition of SNDs in casting solution up to 1.0 wt% decreased the TFR. The lower TFR values represent the better antifouling properties of the membranes. Moreover, lower values of IFR for nanocomposite membranes exhibit that adsorbed foulants on the membrane surface or its pores can be treated by physical treatment. As it mentioned in section 3.2.2 addition of nanoparticles cause reduction in the size of surface pores of the membranes, which acts as a barrier for relatively big HA molecules to penetrate into the pores of the membranes. On the other hand hydrophilic surfaces make stronger bands with water molecules, so the formation of thin water layer on the membrane surface will reduce the hydrophobic adsorption of HA [37, 38]. Table 3 also shows that by addition of SNDs, the

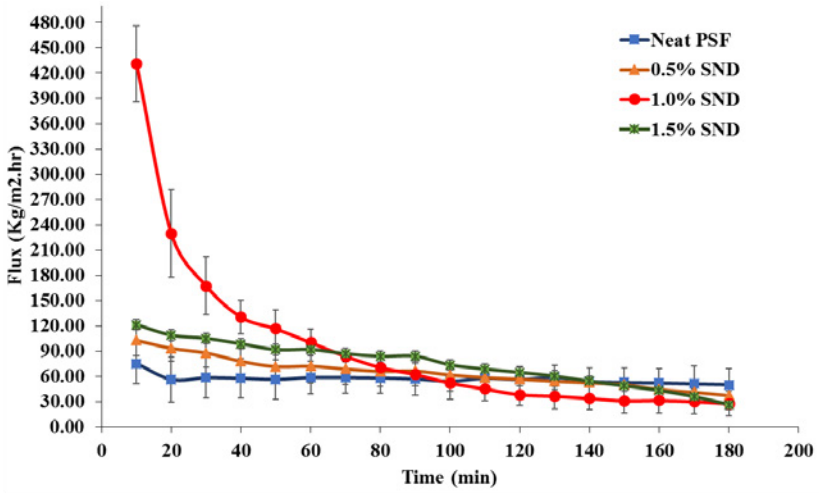

Fig. 6. HA filtration fluxes of different membranes.

Table 3. Fouling and rejection parameters of prepared membranes during HA filtration with and without pre-coagulation process.

Membrane	Without pre-coagulation (%)					With pre-coagulation (%)				
	RFR	IFR	TFR	FRR	R	RFR	IFR	TFR	FRR	R
PSf/SND (0.0 wt%)	2.01	78.01	80.01	21.98	9.02	6.82	53.99	60.81	46.00	97.75
PSf/SND (0.5 wt%)	3.31	67.06	70.37	32.93	30.20	20.45	43.51	63.96	56.48	96.10
PSf/SND (1.0 wt%)	25.75	45.63	71.38	54.36	47.03	64.52	20.09	84.62	79.90	97.89
PSf/SND (1.5 wt%)	29.46	59.64	89.10	40.35	22..88	58.12	33.14	91.26	66.85	97.79

FRR values have increased from 21.98% for neat PSf to 54.36% for PSf/SND (1.0 wt%). FRR is an index indicating the degree of recovery of water flux after cleaning a fouled membrane and higher values of FRR indicates better antifouling property of the ultrafiltration membranes [39]. As expected, RFR values have increased from 2.01% for neat PSf to 25.75% for PSf/SND (1.0 wt%). Consequently. These results are consistent with RFR values and higher RFR corresponds to higher FRR.

As reported by Akbari et al. [40] and Etemadi et al. [15] in coagulation-ultrafiltration process, the addition of coagulants played an important role in improving the antifouling characteristics of membranes. Thus in this study fouling parameters were evaluated after adding of coagulant and the results were depicted in Table 3. Improvements in RFR and FRR were identified in the presence of pre-coagulation process for all samples. Aggregation of HA which resulted from addition of coagulants, can prevent the penetration of small particles into membrane pores and increase FRR.

The effect of coagulation on HA rejection is also shown in Table 3. It is obvious that pre-coagulation with PAC in the filtration of HA with coagulation, the membranes are more effective compared to filtration without pre-coagulation. In the filtration without coagulation, PSf/SND (1.5 wt.%) removed only 47.03% of HA, suggesting that this membrane alone was less effective in HA removal. In the filtration with pre-coagulation, the HA rejection had increased to 97.89%. Coagulants cause to the aggregate of HA and increase the particle size which leads to effective removal of HA.

Fig. 7 shows the fitting of the obtained experimental data after using the neat PSf and nanocomposite membranes to different predicted fouling mechanisms, including complete pore blocking, standard pore blocking, intermediate pore blocking and cake formation. So in order to identify the mechanism of fouling during the HA filtration, the experimental fouling data substituted in linearized equations of Hermia models and k values were estimated by a linear regression method. The adjusted values of k and correlation coefficient; R^2 for the neat and nanocomposite membranes are listed in Table 4.

From Fig. 7 it can be seen that a cake filtration model provides the best fit for nanocomposite membranes except for PSf/SND (1.0 wt%), which

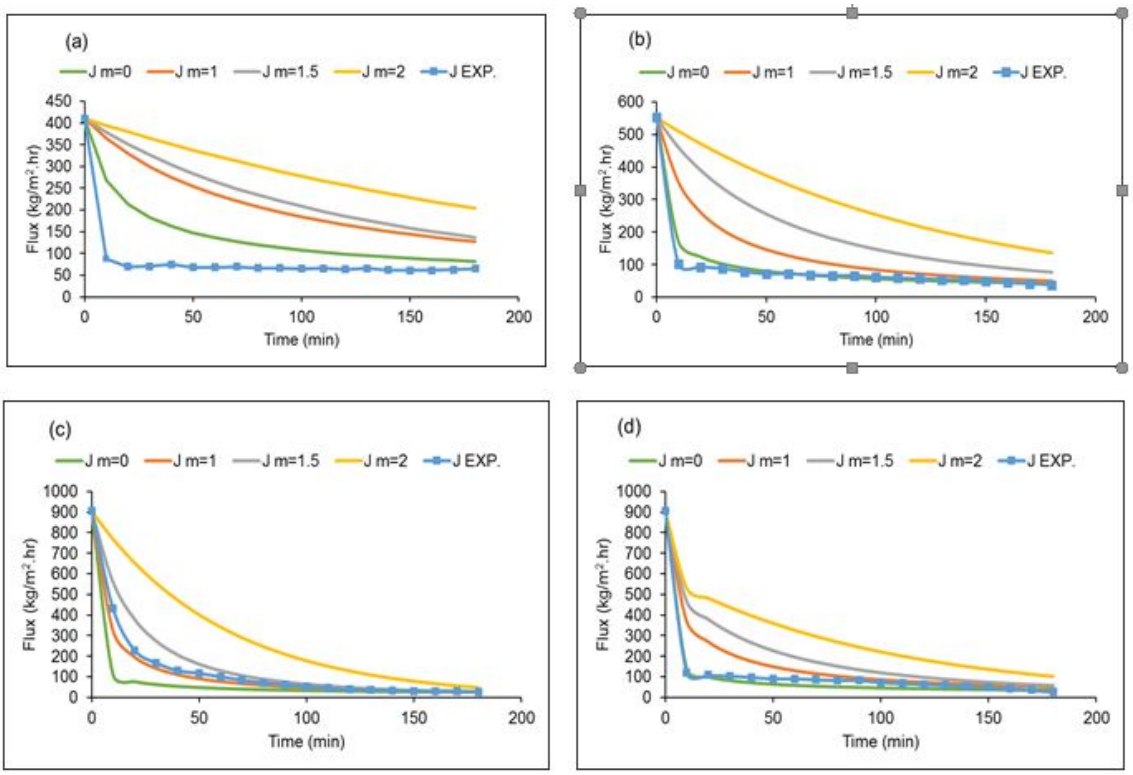

Fig. 7. Experimental data and Hermia fouling models for (a) PSf, (b) PSf/SND (0.5 wt%), (c) PSf/SND (1.0 wt%), (d) PSf/SND (1.5 wt%) membrane during filtration of HA solution.

Table 4. Obtained k and correlation coefficient R^2 values for Hermia fouling models.

Membrane	m=0		m=1		m=1.5		m=2	
	k	R^2	k	R^2	k	R^2	k	R^2
PSf/SND (0.0 wt%)	$8*10^{-7}$	0.552	0.00003	0.4075	0.0002	0.3343	0.0039	0.2717
PSf/SND (0.5 wt%)	$3*10^{-3}$	0.8843	0.0001	0.8962	0.0004	0.7888	0.0078	0.5939
PSf/SND (1.0 wt%)	$8*10^{-6}$	0.9163	0.0002	0.9868	0.0009	0.9787	0.0162	0.8768
PSf/SND (1.5 wt%)	$5*10^{-6}$	0.5921	0.0001	0.8005	0.0005	0.8446	0.0097	0.7394

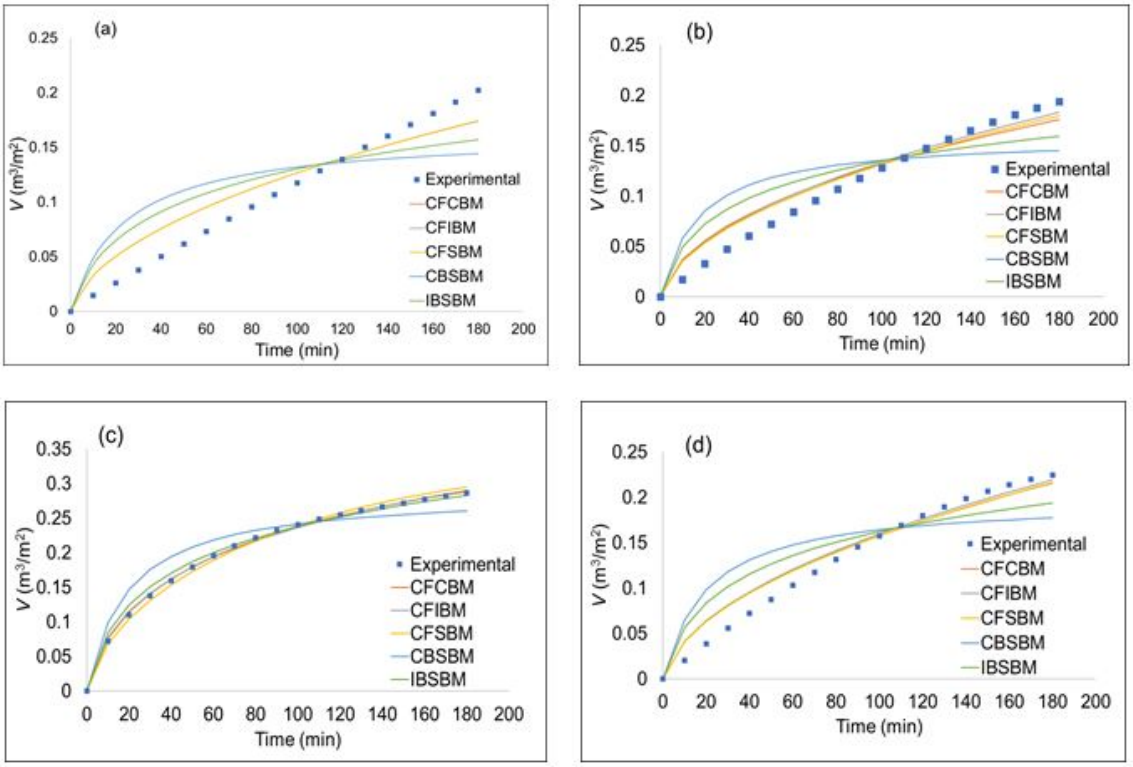

Fig. 8. Experimental filtrated volume data compared to the combined fouling models for (a) PSf, (b) PSf/SND (0.5 wt%), (c) PSf/SND (1.0 wt%), (d) PSf/SND (1.5 wt%) membrane during filtration of HA solution.

is axiomatic due to the use of dead-end filtration system. On the other hand for PSf/SND (1.0 wt%), the best-fitted model is intermediate fouling which means foulants have accumulated on each other and have blocked some pores, but it is considered as reversible fouling and can be removed by physical cleaning so the FRR will increase. However, none of the four classical fouling models was in good agreement with the experimental data of neat PSf membrane and so was not capable of identifying the fouling behavior of the filtration process. Consequently, for more accurate investigation and studying the simultaneous effects of several fouling mechanisms, five combined models according to Table S2 were applied to the HA filtration. The values of fitted parameters, correlation coefficient, R^2 and sum of squared errors (SSE) for neat and nanocomposite membranes are listed in Table 5.

As shown in Fig. 8 it can be seen that for all the membrane except PSf/SND (1.0 wt%), the best fit of the data occurred with the combined cake filtration-standard blocking (CFSBM). However, the best fit of the data for PSf/SND (1.0 wt%) membrane was observed only in the cake filtration-complete blocking (CFCBM). It is interesting to mention that cake filtration and complete blocking are considered as reversible fouling that can be removed by physical cleaning methods and so the FRR will increase. However, the standard blocking is categorized as irreversible fouling because of the accumulation of particles on the walls of the pores of the membrane. That's why PSf/SND (1.0 wt%) membrane has the best-improved fouling parameters like FRR, compared to the others.

Table 5. Model parameters, regression coefficient and error of fit for constant pressure combined models of membrane fouling.

Membrane	Models	R^2	SSE	Fitted parameters
PSf/SND (0.0 wt%)	CFCBM	0.9147	0.006002	k_c=1.02*10^4 min/m^2, k_b= 1*10^{-4} min^{-1}
	CFIBM	0.9135	0.00609	k_c=1*10^4 min/m^2, k_i=1*10^{-1} m^{-1}
	CFSBM	0.9149	0.005987	k_c=1.02*10^4 min/m^2, k_s=0.02607 m^{-1}
	CBSBM	0.6447	0.025	k_b=0.0007357 min^{-1}, k_s=12.14 m^{-1}
	IBSBM	0.7798	0.01549	k_i=20.98 m^{-1}, k_s=6.26*10^{-9} m^{-1}
PSf/SND (0.5 wt%)	CFCBM	0.9372	0.004096	k_c=8.33*10^3 min/m^2, k_b= 1*10^{-2} min^{-1}
	CFIBM	0.9508	0.003207	k_c=9.54*10^3 min/m^2, k_i=8.52*10^{-3} m^{-1}
	CFSBM	0.9524	0.003103	k_c=9.92*10^3 min/m^2, k_s=0.1088 m^{-1}
	CBSBM	0.6485	0.02292	k_b=5.36*10^{-7} min^{-1}, k_s=12.58 m^{-1}
	IBSBM	0.8086	0.01248	k_i=22.92 m^{-1}, k_s=1*10^{-2} m^{-1}
PSf/SND (1.0 wt%)	CFCBM	0.999	0.0001089	k_c=1.26*10^3 min/m^2, k_b=3.56*10^{-2} min^{-1}
	CFIBM	0.9981	0.0002148	k_c=9.51*10^2 min/m^2, k_i=4 m^{-1}
	CFSBM	0.9943	6.39*10^{-4}	k_c=1.91*10^3 min/m^2, k_s=5.41 m^{-1}
	CBSBM	0.9217	0.008744	k_b=3.19*10^{-4} min^{-1}, k_s=6.929m^{-1}
	IBSBM	0.9926	0.0008308	k_i=12.58 m^{-4}, k_s=1*10^{-4} m^{-1}
PSf/SND (1.5 wt%)	CFCBM	0.9588	0.003784	k_c=6.62*10^3 min/m^2, k_b= 1*10^{-3} min^{-1}
	CFIBM	0.9593	0.003741	k_c=6.56*10^3 min/m^2, k_i=2.36*10^{-3} m^{-3}
	CFSBM	0.9601	3.67*10^{-3}	k_c=6.74*10^3 min/m^2, k_s=0.04033 m^{-1}
	CBSBM	0.6968	0.02787	k_b=1.49*10^{-3} min^{-1}, k_s=9.987 m^{-1}
	IBSBM	0.838	0.01489	k_i=18 m^{-1}, k_s=1.78*10^{-7} m^{-1}

CONCLUSION

In this study, PSf nanocomposite membranes by incorporating silanized nanodiamonds were fabricated via NIPS method. The antifouling behavior of neat and nanocomposite PSf membranes during the filtration of HA in the dead-end system was investigated. The fouling characteristics of membranes of fabricated membranes were investigated using Hermia and combined fouling model. The successful silanization of NDs was confirmed by FTIR analysis. Improvement in hydrophilicity, porosity, PWF and mechanical strength of nanocomposite membranes was achieved. According to the fouling results, Hermia's model was unable to identify the fouling behavior of the filtration process. Consequently, with the aid of combined models, it was concluded that the best-fitted data for all the membranes except for PSf/SND (1.0 wt%) is cake filtration-standard blocking (CFCBM) while for the PSf/SND (1.0 wt%) the best-fitted data is cake filtration-complete blocking, which is considered as reversible fouling. Pre-coagulation could increase HA rejection and improve antifouling properties of membranes. Eventually the PSf/SND (1.0 wt%) had the highest values in pure water flux, antifouling properties, hydrophilicity, porosity, and water content, which was due to the presence of more hydrophilic groups on the surface of the membrane. However addition of more than 1.0 wt% SNDs to the polymeric matrix did not represent much improvement in membrane performance because of agglomeration of particles in the composite materials.

CONFLICTS OF INTEREST

There are no conflicts to declare.

REFERENCES

1. Krasner SW, Weinberg HS, Richardson SD, Pastor SJ, Chinn R, Sclimenti MJ, et al. Occurrence of a New Generation of Disinfection Byproducts†. Environmental Science & Technology. 2006;40(23):7175-85.
2. Esfahani MR, Pallem VL, Stretz HA, Wells MJM. Humic acid disaggregation with/of gold nanoparticles: Effects of nanoparticle size and pH. Environmental Nanotechnology, Monitoring & Management. 2016;6:54-63.
3. Zhang Y, Liu F, Lu Y, Zhao L, Song L. Investigation of phosphorylated TiO2–SiO2 particles/polysulfone composite membrane for wastewater treatment. Desalination. 2013;324:118-26.
4. Jhaveri JH, Murthy ZVP. A comprehensive review on anti-fouling nanocomposite membranes for pressure driven membrane separation processes. Desalination. 2016;379:137-54.
5. Shokri E, Yegani R, Pourabbas B, Kazemian N. Preparation and characterization of polysulfone/organoclay adsorptive nanocomposite membrane for arsenic removal from contaminated water. Applied Clay Science. 2016;132-133:611-20.
6. Shokri E, Yegani R, Akbarzadeh A. Novel adsorptive mixed matrix membranes by embedding modified montmorillonite with arginine amino acid into polysulfones for As(V) removal. Applied Clay Science. 2017;144:141-9.
7. Song HJ, Jo YJ, Kim S-Y, Lee J, Kim CK. Characteristics of ultrafiltration membranes fabricated from polysulfone and polymer-grafted silica nanoparticles: Effects of the particle size and grafted polymer on the membrane performance. Journal of Membrane Science. 2014;466:173-82.
8. Phelane L, Muya FN, Richards HL, Baker PGL, Iwuoha EI. Polysulfone Nanocomposite Membranes with improved hydrophilicity. Electrochimica Acta. 2014;128:326-35.

9. Ganesh BM, Isloor AM, Ismail AF. Enhanced hydrophilicity and salt rejection study of graphene oxide-polysulfone mixed matrix membrane. Desalination. 2013;313:199-207.
10. Rezaee R, Nasseri S, Mahvi AH, Nabizadeh R, Mousavi SA, Rashidi A, et al. Fabrication and characterization of a polysulfone-graphene oxide nanocomposite membrane for arsenate rejection from water. Journal of Environmental Health Science and Engineering. 2015;13(1).
11. Kumar M, Gholamvand Z, Morrissey A, Nolan K, Ulbricht M, Lawler J. Preparation and characterization of low fouling novel hybrid ultrafiltration membranes based on the blends of GO–TiO2 nanocomposite and polysulfone for humic acid removal. Journal of Membrane Science. 2016;506:38-49.
12. Wu H, Tang B, Wu P. Development of novel SiO2–GO nanohybrid/polysulfone membrane with enhanced performance. Journal of Membrane Science. 2014;451:94-102.
13. Attia NF, Rao JP, Geckeler KE. Nanodiamond–polymer nanoparticle composites and their thin films. Journal of Nanoparticle Research. 2014;16(4).
14. Javadi M, Jafarzadeh Y, Yegani R, Kazemi S. PVDF membranes embedded with PVP functionalized nanodiamond for pharmaceutical wastewater treatment. Chemical Engineering Research and Design. 2018;140:241-50.
15. Etemadi H, Yegani R, Seyfollahi M. The effect of amino functionalized and polyethylene glycol grafted nanodiamond on anti-biofouling properties of cellulose acetate membrane in membrane bioreactor systems. Separation and Purification Technology. 2017;177:350-62.
16. Liu Y, Gu Z, Margrave JL, Khabashesku VN. Functionalization of Nanoscale Diamond Powder: Fluoro-, Alkyl-, Amino-, and Amino Acid-Nanodiamond Derivatives. Chemistry of Materials. 2004;16(20):3924-30.
17. Jeong M-G, Chun Y-S, Lim D-S, Kim JY. Effect of a silane coupling agent on the optical and the mechanical characteristics of nanodiamond/acrylic resin composites. Journal of the Korean Physical Society. 2014;65(7):1049-53.
18. Dolmatov VY. Composition materials based on elastomer and polymer matrices filled with nanodiamonds of detonation synthesis. Nanotechnologies in Russia. 2009;4(9-10):556-75.
19. Hajiali F, Shojaei A. Silane functionalization of nanodiamond for polymer nanocomposites-effect of degree of silanization. Colloids and Surfaces A: Physicochemical and Engineering Aspects. 2016;506:254-63.
20. Chakrabarty B, Ghoshal AK, Purkait MK. Preparation, characterization and performance studies of polysulfone membranes using PVP as an additive. Journal of Membrane Science. 2008;315(1-2):36-47.
21. Malaisamy R, Mahendran R, Mohan D, Rajendran M, Mohan V. Cellulose acetate and sulfonated polysulfone blend ultrafiltration membranes. I. Preparation and characterization. Journal of Applied Polymer Science. 2002;86(7):1749-61.
22. Jafarzadeh Y, Yegani R, Sedaghat M. Preparation, characterization and fouling analysis of ZnO/polyethylene hybrid membranes for collagen separation. Chemical Engineering Research and Design. 2015;94:417-27.
23. Jafarzadeh Y, Yegani R. Analysis of fouling mechanisms in TiO2 embedded high density polyethylene membranes for collagen separation. Chemical Engineering Research and Design. 2015;93:684-95.
24. Bolton G, Lacasse D, Kuriyel R. Combined models of membrane fouling: Development and application to microfiltration and ultrafiltration of biological fluids. Journal of Membrane Science. 2006;277(1-2):75-84.
25. Etemadi H, Yegani R, Babaeipour V. Study on the reinforcing effect of nanodiamond particles on the mechanical, thermal and antibacterial properties of cellulose acetate membranes. Diamond and Related Materials. 2016;69:166-76.
26. Etemadi H, Yegani R, Babaeipour V. Performance evaluation and antifouling analyses of cellulose acetate/nanodiamond nanocomposite membranes in water treatment. Journal of Applied Polymer Science. 2017;134(21).
27. Aris A, Shojaei A, Bagheri R. Cure Kinetics of Nanodiamond-Filled Epoxy Resin: Influence of Nanodiamond Surface Functionality. Industrial & Engineering Chemistry Research. 2015;54(36):8954-62.
28. Ma L, Cui G, Tao C, Yan H, Hu X. Synthesis and Properties of Polymethyl Methacrylate/Nanodiamond Composite Material. Proceedings of the 2015 International Conference on Electromechanical Control Technology and Transportation: Atlantis Press; 2015.
29. Avilés F, Sierra-Chi CA, Nistal A, May-Pat A, Rubio F, Rubio J. Influence of silane concentration on the silanization of multiwall carbon nanotubes. Carbon. 2013;57:520-9.
30. Teli SB, Molina S, Sotto A, Calvo EG, Abajo Jd. Fouling Resistant Polysulfone–PANI/TiO2 Ultrafiltration Nanocomposite Membranes. Industrial & Engineering Chemistry Research. 2013;52(27):9470-9.
31. Homayoonfal M, Mehrnia MR, Rahmani S, Mohades Mojtahedi Y. Fabrication of alumina/polysulfone nanocomposite membranes with biofouling mitigation approach in membrane bioreactors. Journal of Industrial and Engineering Chemistry. 2015;22:357-67.
32. Jamshidi Gohari R, Lau WJ, Matsuura T, Ismail AF. Fabrication and characterization of novel PES/Fe–Mn binary oxide UF mixed matrix membrane for adsorptive removal of As(III) from contaminated water solution. Separation and Purification Technology. 2013;118:64-72.
33. E. Shoki, R. Yegani, Novel Adsorptive Mixed Matrix Membrane by Incorporating Modified Nanoclay with Amino Acid for Removal of Arsenic from Water, Journal of Water and Environmental Nanotechnology, 2 (2017) 88-95.
34. Chatterjee S, De S. Adsorptive removal of fluoride by activated alumina doped cellulose acetate phthalate (CAP) mixed matrix membrane. Separation and Purification Technology. 2014;125:223-38.
35. Young T-H, Chen L-W. Pore formation mechanism of membranes from phase inversion process. Desalination. 1995;103(3):233-47.
36. Xu Z, Zhang J, Shan M, Li Y, Li B, Niu J, et al. Organosilane-functionalized graphene oxide for enhanced antifouling and mechanical properties of polyvinylidene fluoride ultrafiltration membranes. Journal of Membrane Science. 2014;458:1-13.
37. Arthanareeswaran G, Sriyamunadevi T, Raajenthiren M. Effect of silica particles on cellulose acetate blend

ultrafiltration membranes: Part I. Separation and Purification Technology. 2008;64(1):38-47.
38. Amini M, Etemadi H, Akbarzadeh A, Yegani R. Preparation and performance evaluation of high-density polyethylene/silica nanocomposite membranes in membrane bioreactor system. Biochemical Engineering Journal. 2017;127:196-205.
39. Zinadini S, Zinatizadeh AA, Rahimi M, Vatanpour V, Zangeneh H. Preparation of a novel antifouling mixed matrix PES membrane by embedding graphene oxide nanoplates. Journal of Membrane Science. 2014;453:292-301.
40. Akbari A, Yegani R, Pourabbas B. Synthesis of poly(ethylene glycol) (PEG) grafted silica nanoparticles with a minimum adhesion of proteins via one-pot one-step method. Colloids and Surfaces A: Physicochemical and Engineering Aspects. 2015;484:206-15.